

H_0 Ex Machina: Vacuum Metamorphosis and Beyond H_0

Eleonora Di Valentino*

*Jodrell Bank Center for Astrophysics, School of Physics and Astronomy,
University of Manchester, Oxford Road, Manchester, M13 9PL, UK*

Eric V. Linder†

*Berkeley Center for Cosmological Physics & Berkeley Lab,
University of California, Berkeley, CA 94720, USA and
Energetic Cosmos Laboratory, Nazarbayev University, Astana, Kazakhstan 010000*

Alessandro Melchiorri‡

Physics Department and INFN, Università di Roma “La Sapienza”, Ple Aldo Moro 2, 00185, Rome, Italy

(Dated: July 1, 2020)

We do not solve tensions with concordance cosmology; we do obtain $H_0 \approx 74$ km/s/Mpc from CMB+BAO+SN data in our model, but that is not the point. Discrepancies in Hubble constant values obtained by various astrophysical probes should not be viewed in isolation. While one can resolve at least some of the differences through either an early time transition or late time transition in the expansion rate, these introduce other changes. We advocate a holistic approach, using a wide variety of cosmic data, rather than focusing on one number, H_0 . Vacuum metamorphosis, a late time transition physically motivated by quantum gravitational effects and with the same number of parameters as Λ CDM, can successfully give a high H_0 value from cosmic microwave background data but fails when combined with multiple distance probes. We also explore the influence of spatial curvature, and of a conjoined analysis of cosmic expansion and growth.

I. INTRODUCTION

Considerable literature has been devoted to differences in values for the present cosmic expansion rate, H_0 , obtained by local distance ladder measurements using Cepheid star calibrators [1] or tip of the red giant branch stars [2], by the cosmic microwave background (CMB) data [3, 4], by baryon acoustic oscillation data in conjunction with primordial nucleosynthesis constraints but independent of CMB [5–7], and by strong gravitational lensing time delays [8]. We do not opine here on the possibility of inaccurate measurements or techniques (systematics) but instead pursue the avenue of actual new cosmic physics: the fault is not in our stars, but in ourselves (i.e. cosmological model).

Two modifications of cosmological history have long been known as capable of raising the value determined by probes for the present expansion rate: an early time transition in the expansion rate (e.g. through adding extra energy density), thus decreasing the sound horizon [9–13], and a late time transition in the expansion rate (through either adding extra energy density or changing the Friedmann equation relating expansion rate to energy density), thus directly raising H_0 [14–19].

Each of these, however, have other cosmological effects besides changing H_0 , e.g. on distances, the value of the matter density Ω_m , CMB anisotropies, the amplitude or rate of growth of structure ($\sigma_8, f\sigma_8, S_8$). For example, early time transitions must quickly shed their extra energy density so as not to disrupt the fit to CMB anisotropies or cosmic structure formation. Indeed, [13] actually detected such a transition up and down in the Planck 2013 and WMAP9 CMB data and showed the shift in H_0 . Recently this idea has been revisited by [20–24]. Late time transitions that raise H_0 generally lower Ω_m (e.g. if keeping the well measured value of $\Omega_m h^2$), changing distances to sources, the growth of structure, and generally also the sound horizon and CMB anisotropies. Some of these can be compensated for with other changes but it is difficult to match all the data. Recent treatments of early time transitions [25] and late time transitions [26] highlight some of the issues, while the overall situation is summarized in [27]. There are a huge number of papers discussing specific aspects and models: we refer the reader to references in [27] as well as more recent ones that evaluate viability with respect to multiple, diverse data sets [28–51].

Here we address a late time transition in fundamental physics, arising from the well motivated quantum gravity effect of Parker’s vacuum metamorphosis [52–54]. This follows on the early attempt to use vacuum metamorphosis to attain higher H_0 in [14], which was successful for the probes considered. We emphasize that this is a first principles

* eleonora.divalentino@manchester.ac.uk

† evlinder@lbl.gov

‡ alessandro.melchiorri@roma1.infn.it

theory, not a phenomenological parametrization. A theory with a similar transition but different origin is übergravity [18]. We will go beyond these works by exploring the role of spatial curvature and adding further observational probes.

Section II describes the vacuum metamorphosis theory in both its original and VEV forms, with the same and one more number of parameters as Λ CDM, respectively. In Sec. III we present the data sets we will use in different combinations. Section IV discusses the cosmological constraints including on H_0 and the spatial curvature, paying close attention to goodness of fit. We highlight in Sec. V the importance of using a wide range of different robust probes, and effects on cosmic structure growth, including a conjoined analysis. We discuss general lessons about late time transitions and conclude in Sec. VI.

II. VACUUM METAMORPHOSIS

Vacuum metamorphosis arises from a nonperturbative summation of quantum gravity loop corrections due to a massive scalar field. The first order loop correction is familiar as Starobinsky R^2 gravity [55], where R is the Ricci scalar. When the Ricci scalar evolves during cosmic history to reach the scalar field mass squared, then a phase transition occurs and R freezes with $R = m^2$. This changes the expansion rate from the earlier time, pure matter evolution. That is, at times before the phase transition the action is purely of the Einstein-Hilbert form without any dark energy, while at later times the cosmic expansion has a different evolution. Other theories giving a phase transition in R include Sakharov's induced gravity [56] and the sum over states approach of übergravity [18].

Vacuum metamorphosis is a highly predictive theory, as it has the same number of parameters as Λ CDM. In the original form there is a relation between m^2 and the present matter density Ω_m (which also determines the transition redshift). Another possible form is where the massive scalar field has a vacuum expectation value (VEV) that manifests as a cosmological constant at higher redshift – thus the cosmology at earlier times than the transition is purely Λ CDM. Here the VEV, or magnitude of the high redshift cosmological constant, is another free parameter. We will explore the constraints of the data on both the original and VEV forms of vacuum metamorphosis.

We now review the key equations of vacuum metamorphosis (VM), extending them to include spatial curvature, and discussing our implementation of them. While we regard the original VM model without cosmological constant as the most elegant and theoretically compelling, we provide the general equations for the VEV form, with the original no high redshift cosmological constant form as a special case.

The phase transition criticality condition is

$$R = 6(\dot{H} + 2H^2 + ka^{-2}) = m^2, \quad (1)$$

and, defining $M = m^2/(12H_0^2)$, the expansion behavior above and below the phase transition is

$$H^2/H_0^2 = \Omega_m(1+z)^3 + \Omega_r(1+z)^4 + \Omega_k(1+z)^2 + M \left\{ 1 - \left[3 \left(\frac{4}{3\Omega_m} \right)^4 M(1-M-\Omega_k-\Omega_r)^3 \right]^{-1} \right\}, \quad z > z_t \quad (2)$$

$$H^2/H_0^2 = (1-M-\Omega_k)(1+z)^4 + \Omega_k(1+z)^2 + M, \quad z \leq z_t \quad (3)$$

where $\Omega_k = -k/H_0^2$ is the spatial curvature effective energy density and Ω_r is the radiation energy density. The phase transition occurs at

$$z_t = -1 + \frac{3\Omega_m}{4(1-M-\Omega_k-\Omega_r)}. \quad (4)$$

We see that above the phase transition, the universe behaves as one with matter (plus radiation plus spatial curvature) plus a cosmological constant, and after the phase transition it effectively has a radiation component (the matter and usual radiation is hidden within this expression) that rapidly redshifts away leaving a de Sitter phase. The original model did not include a VEV; we see that this lack of an explicit high redshift cosmological constant implies that

$$\Omega_m = \frac{4}{3} [3M(1-M-\Omega_k-\Omega_r)^3]^{1/4}. \quad (\text{no VEV case}) \quad (5)$$

So there is only one free parameter in the original model, either M or Ω_m , the same number as in Λ CDM. For example, $\Omega_m = 0.3$ implies $M = 0.9017$, and $z_t = 1.29$. We emphasize that the de Sitter behavior at late times is not a result of a cosmological constant, but rather the intrinsic physics of the model.

The effective dark energy equation of state (i.e. of the effective component once the matter and normal radiation contributions have been accounted for) is

$$w(z) = -1 - \frac{1}{3} \frac{3\Omega_m(1+z)^3 - 4(1-M-\Omega_k-\Omega_r)(1+z)^4}{M + (1-M-\Omega_k-\Omega_r)(1+z)^4 - \Omega_m(1+z)^3}, \quad (6)$$

below the phase transition, and simply $w(z > z_t) = -1$ above the phase transition. In the case without a cosmological constant (no VEV), there is no dark energy above the transition.

The equation of state behavior is phantom, and more deeply phantom as the VEV diminishes. Note that for $M > 0.9017$ (in the $\Omega_m = 0.3$ case), the VEV can go negative, and this leads initially to a highly positive equation of state just after the transition. This is not an observationally viable region. As M falls below the critical value, the VEV smooths out the rapid time variation, leading to a nearly constant $w(a)$. If M falls too low, then the transition occurs in the future (see Eq. 4), and we have simply the Λ CDM model for the entire history to the present. Moreover, M then becomes no longer a free parameter but is given in terms of Ω_m by the requirement that $H(z=0)/H_0 = 1$. Thus, when considering the VM VEV model one would need to place lower and upper limits on the prior of the extra free parameter, corresponding to $z_t \geq 0$ and $\Omega_{\text{de}}(z > z_t) \geq 0$ respectively.

The lower bound on M from Eq. (4) is

$$M_{\text{lower}} = 1 - \frac{3\Omega_m}{4} - \Omega_k - \Omega_r. \quad (7)$$

Determining the upper bound on M , i.e. the nonnegativity of the curly brackets in Eq. (2), requires solving a quartic equation. Therefore we instead choose M as our free parameter and place the prior bounds on Ω_m , for which there is an explicit analytic solution. In this case the bounds on Ω_m become

$$\frac{4}{3}(1-M-\Omega_k-\Omega_r) \leq \Omega_m \leq \frac{4}{3} [3M(1-M-\Omega_k-\Omega_r)^3]^{1/4}, \quad (8)$$

where the lower bound corresponds to the condition $z_t \geq 0$ and the upper bound to $\Omega_{\text{de}}(z > z_t) \geq 0$.

III. DATA

In order to constrain the VM model parameters, we utilize various combinations of some of the most recent cosmological measurements available:

- **CMB:** Temperature and polarization CMB angular power spectra of the Planck legacy release 2018 *plikTT-TEEE+lowl+lowE* [3, 57]. This serves as our baseline data set and is included in all data combinations.
- **CMB lensing:** CMB lensing reconstruction power spectrum data 2018, obtained with a CMB trispectrum analysis in [58]. This data is only included in cases where it is specifically listed.
- **BAO:** Baryon Acoustic Oscillation measurements 6dFGS [59], SDSS MGS [60], and BOSS DR12 [61], in the same combination used by the Planck collaboration in [3].
- **SN:** Luminosity distance data of 1048 Type Ia Supernovae from the Pantheon catalog [62].
- **R19:** Gaussian prior $H_0 = 74.03 \pm 1.42$ km/s/Mpc at 68% CL on the Hubble constant as measured by the SH0ES collaboration in [1].

We assume initially a 6-dimensional parameter space, varying at the same time the baryon energy density $\Omega_b h^2$, the ratio of the sound horizon at decoupling to the angular diameter distance to last scattering θ_{MC} , the optical depth to reionization τ , the amplitude and the spectral index of the primordial scalar perturbations A_s and n_s , and the vacuum metamorphosis parameter M defined in Sec. II and related to the matter density Ω_m through the Eq. (5). A second set of analyses includes the curvature density Ω_k , i.e. a spatially nonflat universe, as a seventh parameter. Each of these sets is then also analyzed for the VM VEV model where one more degree of freedom is present, i.e. relaxing the condition of Eq. (5), and also allowing the cold dark matter density $\Omega_c h^2$, equivalent to Ω_m independent of M , to vary. We use flat uniform priors on these parameters, as reported in Table I.

In order to study the data and evaluate the constraints on the cosmological parameters, we use our modified version of the publicly available Monte-Carlo Markov Chain package *CosmoMC* [63], equipped with a convergence diagnostic based on the Gelman and Rubin statistic [64], implementing an efficient sampling of the posterior distribution that makes use of the fast/slow parameter decorrelations [65]. *CosmoMC* includes the support for the 2018 Planck data release [57] (see <http://cosmologist.info/cosmomc/>).

Parameter	Prior
$\Omega_b h^2$	[0.005, 0.1]
$\Omega_c h^2$	[0.001, 0.99]
τ	[0.01, 0.8]
n_s	[0.8, 1.2]
$\log[10^{10} A_s]$	[1.6, 3.9]
$100\theta_{MC}$	[0.5, 10]
M	[0.5, 1]
Ω_k	[-0.3, 0.3]

Table I. Flat priors adopted for the cosmological parameters.

IV. COSMOLOGICAL CONSTRAINTS

Cosmological parameter constraints are summarized in Table II and III for the original VM case with no high redshift cosmological constant, i.e. no vacuum expectation value “noVEV”. Table III includes spatial curvature Ω_k as a fit parameter. The 68% and 95% marginalized confidence level parameter contours and 1D PDFs are shown in Fig. 1 and Fig. 2, respectively. Analogously, the VM VEV model results are presented in Table IV for the VM VEV flat case and in Table V for the VM VEV curvature case, with Fig. 3 and Fig. 4 showing the parameter contours and PDFs.

A. General Results

The first result we note is that the values of H_0 obtained in the VM model are significantly higher than in Λ CDM, with values of $H_0 \approx 73 - 74$ readily reached. Even though VM noVEV has the same number of parameters as Λ CDM, the uncertainty on the H_0 determination from CMB alone is considerably higher: the equivalent CMB TTTEEE only constraint in Λ CDM is $H_0 = 67.27 \pm 0.60$.

A similar trend in the size of the H_0 uncertainty exists within w CDM (with one extra parameter), where the uncertainty nearly fills the priors. Thus Λ CDM is a special case regarding the level of tension in H_0 for CMB data alone. If we include both BAO and SN data, then the uncertainty recedes to 0.66 (for VM noVEV flat), compared to 0.43 for Λ CDM, and the mean value $H_0 = 74.21$ is quite consistent with R19, even though we did not use a R19 prior, while it is $H_0 = 67.74$ for Λ CDM.

The five standard cosmological fit parameters are basically the same for VM noVEV and Λ CDM, but derived parameters such as Ω_m and σ_8 , in addition to H_0 , can be quite different. Therefore it is important to examine the overall fit to the data, not just look at a single parameter. We compare the best fit χ^2 values of each combination of data used, between VM noVEV flat and Λ CDM (where the number of parameters are equal), between VM noVEV flat and VM noVEV curvature (with one extra parameter, Ω_k), and between VM noVEV curvature and Λ CDM+ Ω_k (with the same number of parameters). We have also checked individual contributions to the χ^2 , e.g. from low ℓ CMB data (which agrees well with the respective Λ CDM χ^2 values).

Relative to Λ CDM, the VM noVEV flat model (Table II and Fig. 1) has moderate improvements in χ^2 for CMB data, a strong improvement for CMB+R19, but much worse fits for CMB with BAO or SN. When both models allow for curvature (Table III and Fig. 2), the CMB only fit becomes slightly worse, and the fits with BAO or SN improve significantly, but not enough to overtake Λ CDM+ Ω_k . And the combination CMB+BAO+SN shows significant tension, as we discuss in Sec. IV B. Thus focusing only on H_0 gives a very biased view of the usefulness of a cosmological model. Within the VM noVEV models, the addition of curvature has a moderate improvement relative to the VM noVEV flat case for the CMB only fit, a strong to very strong effect on the CMB with BAO or R19 or SN sets, and a significant effect on CMB+BAO+SN ($\Delta\chi^2 = -10$ for one extra parameter). In this last combination the preference for a closed universe is 2.9σ , but again this model is a worse fit than Λ CDM+ Ω_k – which is consistent with flatness – by $\Delta\chi^2 = 85$. The CMB+SN case prefers a quite distinct part of the posterior, and so while its fit is reasonable, the combination with BAO is emphatically not. The fit with CMB+BAO+R19 has relative $\Delta\chi^2 = -83$ with respect to CMB+BAO+SN when each is compared to the corresponding Λ CDM+ Ω_k case. Thus the VM noVEV model, whether flat or with curvature, though it does naturally give H_0 consistent with R19, cannot simultaneously satisfy CMB, BAO, and SN data.

Moving to the VM VEV model, we present the results in Table IV and Fig. 3 for the VM VEV flat case and Table V and Fig. 4 for the VM VEV curvature case. The addition of one parameter for the VEV (i.e. both M and $\Omega_c h^2$ or effectively Ω_m free) has an insignificant effect relative to VM noVEV for CMB only, a strong effect for CMB with BAO

Table II. 68% CL constraints on the cosmological parameters for the different dataset combinations explored in this work. This is for the original VM case and spatial flatness: VM noVEV flat. $\Delta\chi_{\text{bf}}^2$ (best fit) is relative to the corresponding data best fits within Λ CDM.

Parameters	CMB	CMB+lensing	CMB+BAO	CMB+Pantheon	CMB+R19	CMB+BAO+Pantheon	CMB+BAO+R19
$\Omega_b h^2$	0.02238 ± 0.00014	0.02242 ± 0.00013	0.02218 ± 0.00012	0.02201 ± 0.00013	0.02221 ± 0.00012	0.02213 ± 0.00012	0.02217 ± 0.00012
$100\theta_{MC}$	1.04091 ± 0.00030	1.04097 ± 0.00029	1.04060 ± 0.00029	1.04033 ± 0.00031	1.04063 ± 0.00029	1.04053 ± 0.00029	1.04060 ± 0.00029
τ	0.0524 ± 0.0078	0.0510 ± 0.0078	$0.0458^{+0.0083}_{-0.0067}$	$0.039^{+0.010}_{-0.007}$	0.0469 ± 0.0075	$0.0449^{+0.0079}_{-0.0065}$	$0.0456^{+0.0083}_{-0.0068}$
M	$0.9363^{+0.0055}_{-0.0044}$	0.9406 ± 0.0034	0.9205 ± 0.0023	$0.8996^{+0.0081}_{-0.0073}$	$0.9230^{+0.0042}_{-0.0036}$	0.9163 ± 0.0023	0.9198 ± 0.0020
$\ln(10^{10} A_s)$	3.041 ± 0.016	3.036 ± 0.015	$3.035^{+0.017}_{-0.014}$	$3.027^{+0.020}_{-0.014}$	3.036 ± 0.016	$3.035^{+0.017}_{-0.014}$	$3.035^{+0.017}_{-0.015}$
n_s	0.9643 ± 0.0039	0.9663 ± 0.0036	0.9572 ± 0.0031	0.9511 ± 0.0036	0.9585 ± 0.0033	0.9560 ± 0.0031	0.9571 ± 0.0031
H_0 [km/s/Mpc]	81.1 ± 2.1	82.9 ± 1.5	75.44 ± 0.69	70.1 ± 1.8	76.3 ± 1.2	74.21 ± 0.66	75.22 ± 0.60
σ_8	0.9440 ± 0.0077	0.9392 ± 0.0067	$0.9456^{+0.0082}_{-0.0070}$	$0.9419^{+0.0098}_{-0.0069}$	0.9457 ± 0.0075	$0.9461^{+0.0080}_{-0.0068}$	$0.9457^{+0.0082}_{-0.0073}$
S_8	0.805 ± 0.022	0.783 ± 0.014	0.865 ± 0.010	0.927 ± 0.023	0.856 ± 0.015	0.880 ± 0.010	0.8675 ± 0.0098
Ω_m	$0.218^{+0.010}_{-0.012}$	0.2085 ± 0.0076	0.2510 ± 0.0046	0.291 ± 0.015	$0.2458^{+0.0074}_{-0.0084}$	0.2593 ± 0.0046	0.2525 ± 0.0040
χ_{bf}^2	2767.74	2776.23	2806.22	3874.13	2777.04	3910.01	2808.34
$\Delta\chi_{\text{bf}}^2$	-4.91	-5.81	+26.51	+66.63	-14.80	+95.83	+11.29

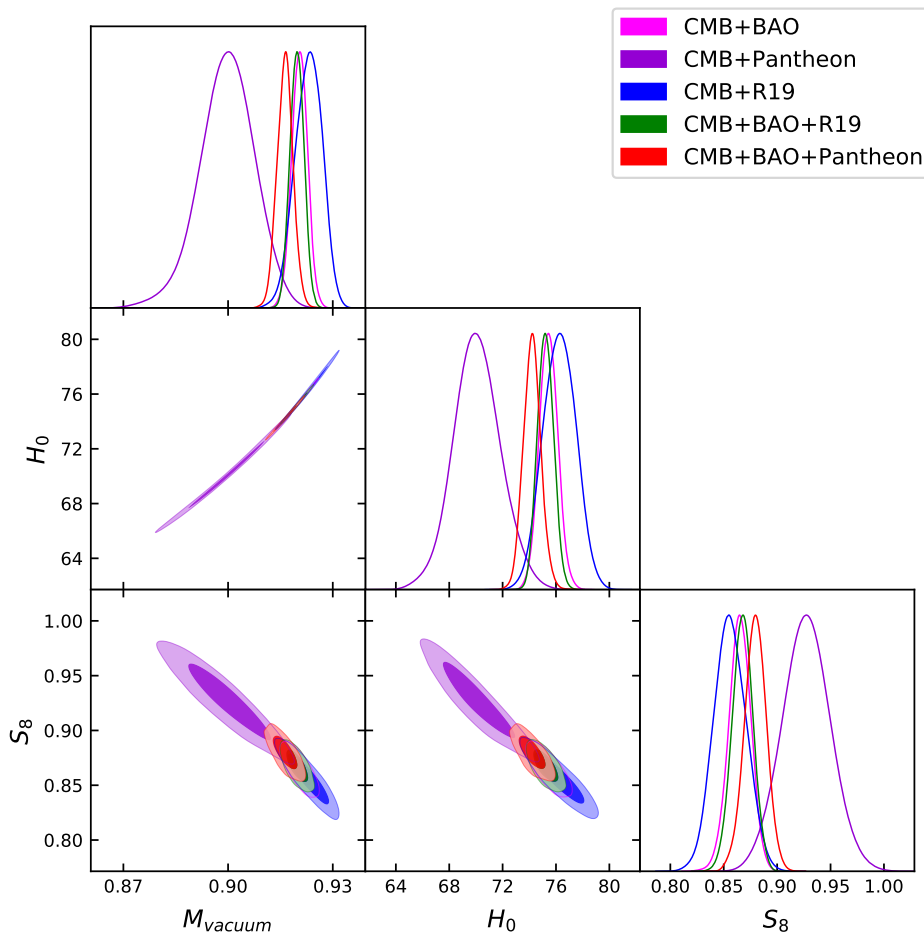


Figure 1. 68% and 95% CL constraints on the original VM case and spatial flatness: VM noVEV flat.

or SN, and a highly significant effect for the combination CMB+BAO+SN ($\Delta\chi^2 = -53$ for one extra parameter). The VM VEV model brings $H_0 \approx 73$, $\Omega_m \approx 0.27$, and $S_8 \approx 0.83$, whether flat or with curvature. Relative to Λ CDM, the VM VEV flat model has $\Delta\chi^2 = +43$ with one extra parameter for CMB+BAO+SN. Note that [66] also showed the tension of fitting CMB+BAO+SN simultaneously (for the data at that time), where in their Fig. 6 the SN contour curves away from the others as one reduces the VM VEV case to VM noVEV, so the SN data play a particularly important discriminating role. While the fit with CMB+BAO+R19 actually has an improved fit relative to Λ CDM,

Table III. As Table II but also allowing spatial curvature to vary, i.e. VM noVEV curvature.

Parameters	CMB	CMB+lensing	CMB+BAO	CMB+Pantheon	CMB+R19	CMB+BAO+Pantheon	CMB+BAO+R19
$\Omega_b h^2$	0.02263 ± 0.00017	0.02250 ± 0.00016	0.02251 ± 0.00016	0.02275 ± 0.00016	0.02254 ± 0.00016	0.02239 ± 0.00015	0.02250 ± 0.00016
$100\theta_{MC}$	1.04119 ± 0.00032	1.04107 ± 0.00032	1.04105 ± 0.00033	1.04130 ± 0.00033	1.04111 ± 0.00031	1.04092 ± 0.00031	1.04105 ± 0.00032
τ	$0.0486^{+0.0084}_{-0.0075}$	0.0498 ± 0.0083	0.0511 ± 0.0075	$0.0391^{+0.0011}_{-0.0007}$	0.0512 ± 0.0079	$0.0483^{+0.0079}_{-0.0067}$	0.0513 ± 0.0075
Ω_k	$-0.030^{+0.016}_{-0.011}$	$-0.0044^{+0.0064}_{-0.0052}$	-0.0128 ± 0.0039	$-0.073^{+0.012}_{-0.010}$	-0.0149 ± 0.0044	-0.0110 ± 0.0038	-0.0127 ± 0.0037
M	$0.927^{+0.010}_{-0.007}$	0.9416 ± 0.0037	0.9336 ± 0.0044	$0.8993^{+0.0094}_{-0.0083}$	0.9340 ± 0.0050	0.9277 ± 0.0044	0.9333 ± 0.0043
$\ln(10^{10} A_s)$	$3.028^{+0.018}_{-0.016}$	3.031 ± 0.018	3.035 ± 0.015	$3.006^{+0.023}_{-0.014}$	3.034 ± 0.016	$3.033^{+0.016}_{-0.014}$	3.036 ± 0.016
n_s	0.9711 ± 0.0047	0.9687 ± 0.0047	0.9684 ± 0.0045	0.9743 ± 0.0046	0.9692 ± 0.0045	0.9648 ± 0.0043	0.9680 ± 0.0044
H_0 [km/s/Mpc]	$67.8^{+4.9}_{-5.4}$	81.0 ± 3.1	74.30 ± 0.74	$55.4^{+1.6}_{-1.8}$	73.7 ± 1.3	73.30 ± 0.72	74.25 ± 0.67
σ_8	$0.903^{+0.022}_{-0.018}$	0.931 ± 0.013	0.9259 ± 0.0091	$0.848^{+0.015}_{-0.014}$	0.9226 ± 0.0098	0.9284 ± 0.0094	0.9262 ± 0.0093
S_8	0.925 ± 0.053	0.795 ± 0.022	0.8609 ± 0.0099	1.060 ± 0.022	0.866 ± 0.015	0.875 ± 0.010	0.8616 ± 0.0097
Ω_m	$0.318^{+0.040}_{-0.055}$	$0.219^{+0.015}_{-0.018}$	0.2594 ± 0.0052	0.469 ± 0.030	$0.264^{+0.009}_{-0.010}$	0.2663 ± 0.0053	0.2597 ± 0.0047
χ^2_{bf}	2762.63	2777.66	2795.27	3811.16	2763.16	3899.96	2795.92
$\Delta\chi^2_{\text{bf}}$	+2.54	+1.60	+18.29	+3.94	-19.84	+85.48	+2.45

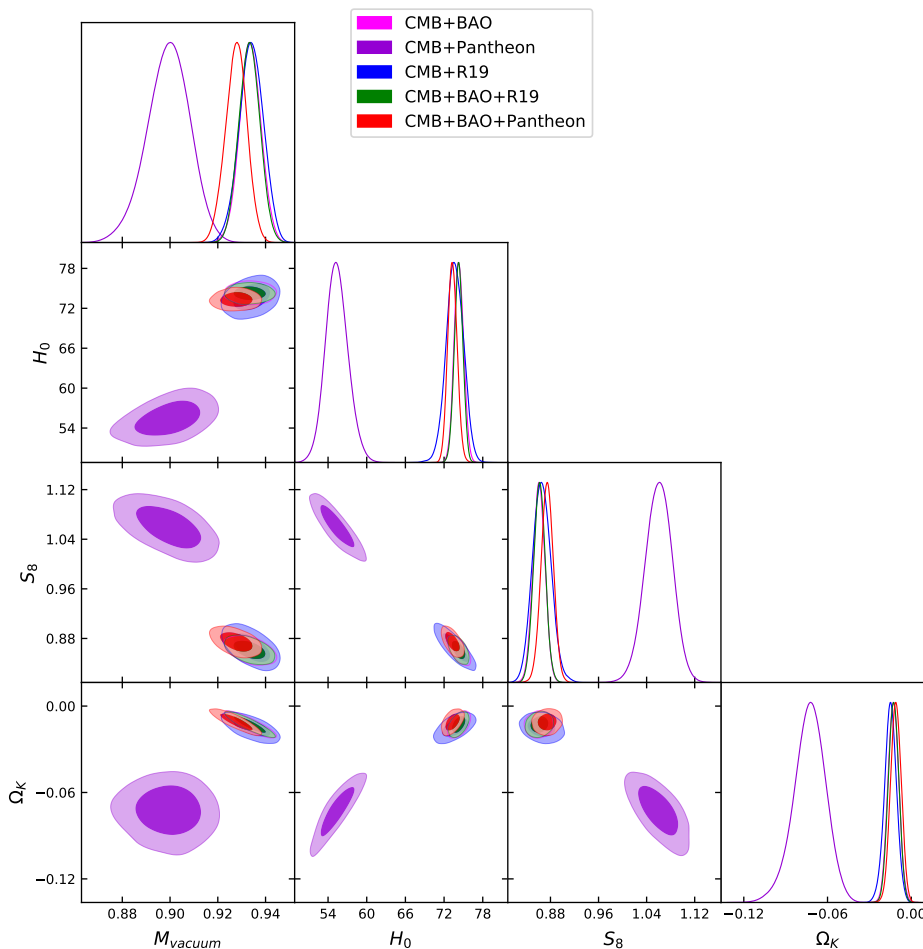


Figure 2. 68% and 95% CL constraints on the original VM case allowing spatial curvature to vary, i.e. VM noVEV curvature.

this comes at the price of neglecting the SN constraints; we discuss this further in Sec. IV B.

Within the VM VEV model, the addition of curvature has a modest effect, except a strong improvement for CMB+SN (simply due to curvature washing out a great part of SN's probative power suppressing one of posterior peaks discussed in Sec. IV B). However, CMB+BAO+SN (and CMB+BAO+R19) shows insignificant change. CMB, CMB+BAO, and CMB+SN all prefer a closed universe but this reduces to a $\sim 1\sigma$ effect for CMB+BAO+SN. For VM VEV curvature relative to $\Lambda\text{CDM}+\Omega_k$, $\Delta\chi^2 = +40$. Removing the SN information gives results relative to $\Lambda\text{CDM}+\Omega_k$ of $\Delta\chi^2 = +10$ for CMB+BAO and -6 for CMB+BAO+R19. Note that adding R19 does not particularly improve

Table IV. As Table II but for the VM VEV model, i.e. VM VEV flat.

Parameters	CMB	CMB+lensing	CMB+BAO	CMB+Pantheon	CMB+R19	CMB+BAO+Pantheon	CMB+BAO+R19
$\Omega_b h^2$	0.02238 ± 0.00015	0.02242 ± 0.00015	0.02229 ± 0.00014	0.02233 ± 0.00015	0.02236 ± 0.00015	0.02228 ± 0.00014	0.02230 ± 0.00014
$\Omega_c h^2$	0.1200 ± 0.0013	0.1194 ± 0.0012	0.1213 ± 0.0012	0.1208 ± 0.0014	0.1203 ± 0.0014	0.1217 ± 0.0012	0.1212 ± 0.0011
$100\theta_{MC}$	1.04092 ± 0.00031	1.04098 ± 0.00030	1.04079 ± 0.00030	1.04086 ± 0.00031	1.04090 ± 0.00032	1.04077 ± 0.00030	1.04080 ± 0.00031
τ	0.0541 ± 0.0078	0.0529 ± 0.0076	0.0527 ± 0.0077	0.0529 ± 0.0077	0.0537 ± 0.0079	0.0524 ± 0.0078	0.0530 ± 0.0077
M	$0.914^{+0.021}_{-0.009}$	$0.920^{+0.017}_{-0.007}$	$0.8950^{+0.0013}_{-0.0033}$	$0.8940^{+0.0012}_{-0.0022}$	$0.9028^{+0.0046}_{-0.0085}$	$0.8929^{+0.0010}_{-0.0016}$	$0.8953^{+0.0014}_{-0.0034}$
$\ln(10^{10} A_s)$	3.044 ± 0.016	3.039 ± 0.015	3.044 ± 0.016	3.043 ± 0.016	3.044 ± 0.016	3.044 ± 0.016	3.045 ± 0.016
n_s	0.9653 ± 0.0044	0.9666 ± 0.0040	0.9620 ± 0.0041	0.9632 ± 0.0025	0.9644 ± 0.0044	0.9612 ± 0.0040	0.9623 ± 0.0038
H_0 [km/s/Mpc]	$76.7^{+3.9}_{-2.6}$	$78.0^{+3.2}_{-1.9}$	$73.58^{+0.33}_{-0.49}$	$73.53^{+0.37}_{-0.42}$	$74.8^{+0.7}_{-1.2}$	73.26 ± 0.32	$73.63^{+0.33}_{-0.48}$
σ_8	$0.895^{+0.016}_{-0.026}$	$0.900^{+0.024}_{-0.019}$	0.876 ± 0.010	0.872 ± 0.010	$0.880^{+0.012}_{-0.016}$	0.8756 ± 0.0091	$0.8760^{+0.0093}_{-0.0099}$
S_8	0.805 ± 0.016	$0.796^{+0.013}_{-0.015}$	0.825 ± 0.014	0.821 ± 0.015	0.813 ± 0.015	0.830 ± 0.013	0.825 ± 0.013
Ω_m	$0.243^{+0.017}_{-0.025}$	$0.235^{+0.011}_{-0.020}$	$0.2664^{+0.0048}_{-0.0043}$	0.2661 ± 0.0050	$0.2561^{+0.0081}_{-0.0068}$	0.2695 ± 0.0041	0.2660 ± 0.0044
χ^2_{bf}	2769.74	2778.93	2790.75	3840.55	2772.09	3857.21	2789.76
$\Delta\chi^2_{\text{bf}}$	-2.91	-3.11	+11.04	+33.05	-19.75	+43.03	-7.29

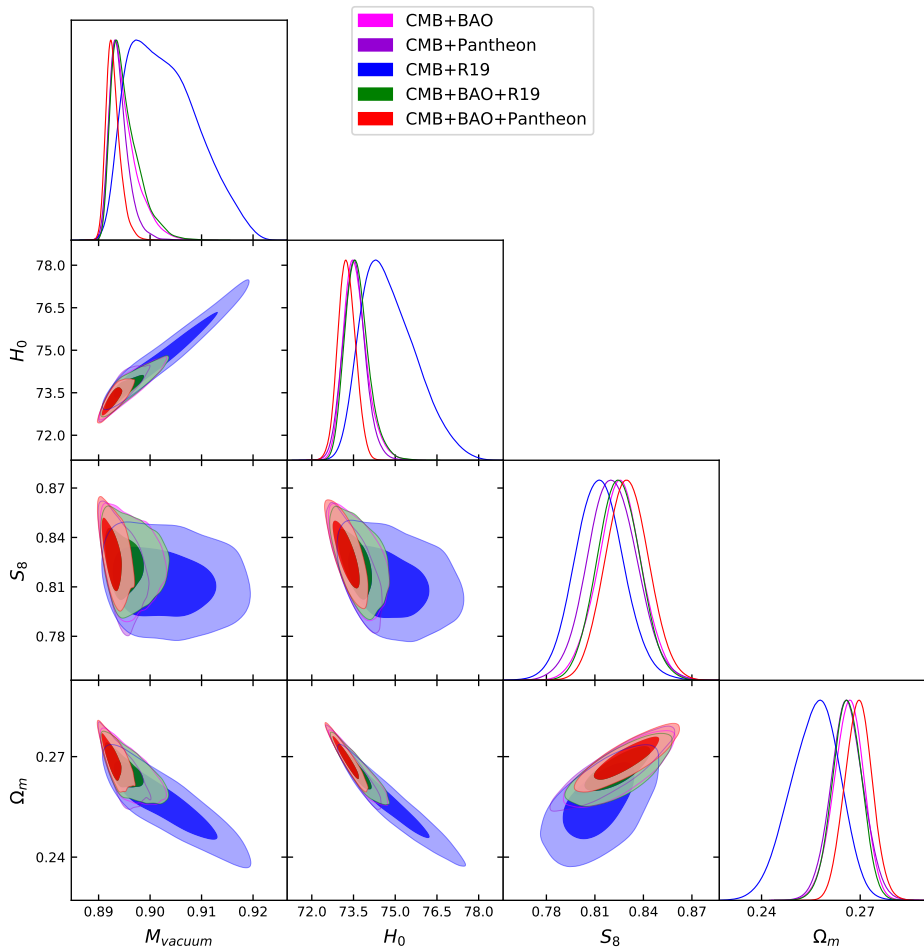


Figure 3. 68% and 95% CL constraints on the VM VEV model, i.e. VM VEV flat.

the VM VEV fit – for one extra data point $\Delta\chi^2 = +0.5$ – but the apparent gain is caused by the $\Lambda\text{CDM}+\Omega_k$ fit getting worse by 16.

Thus, while the VM model can relieve the tension between CMB data and the R19 local Cepheid distance ladder measurement of H_0 , it is not as good a fit to cosmology across a wider combination of data sets including BAO or SN or both. The need for a wide range of probes, including growth ones, will be the main theme of Sec. V, but first we examine apparent sources of tension between CMB+BAO and CMB+SN, and summarize the constraints on H_0 and Ω_k .

Table V. As Table IV but also allowing spatial curvature to vary, i.e. VM VEV curvature. Italicized entries involving Pantheon data serve as a reminder that the parameter values are the mean over both peaks in the posterior; a prior such as $H_0 \gtrsim 60$ would select the peak that is much more consistent with the other data though it does not much affect the total χ^2 values.

Parameters	CMB	CMB+lensing	CMB+BAO	CMB+Pantheon	CMB+R19	CMB+BAO+Pantheon	CMB+BAO+R19
$\Omega_b h^2$	0.02262 \pm 0.00016	0.02248 \pm 0.00016	0.02243 \pm 0.00015	0.02261 \pm 0.00017	0.02251 \pm 0.00016	0.02235 \pm 0.00015	0.02243 \pm 0.00016
$\Omega_c h^2$	0.1180 \pm 0.0015	0.1187 \pm 0.0015	0.1196 \pm 0.0014	0.1181 ^{+0.0015} _{-0.0017}	0.1188 \pm 0.0014	0.1207 \pm 0.0014	0.1197 \pm 0.0014
$100\theta_{MC}$	1.04119 \pm 0.00033	1.04105 \pm 0.00032	1.04098 \pm 0.00031	1.04118 \pm 0.00033	1.04104 ^{+0.00035} _{-0.00030}	1.04086 \pm 0.00032	1.04097 \pm 0.00032
τ	0.0482 \pm 0.0080	0.0506 \pm 0.0080	0.0537 \pm 0.0075	0.0480 ^{+0.0082} _{-0.0071}	0.0519 \pm 0.0076	0.0528 \pm 0.0077	0.0537 \pm 0.0079
Ω_k	-0.040 \pm 0.014	-0.0034 \pm 0.0043	-0.0045 ^{+0.0027} _{-0.0021}	-0.035 ^{+0.005} _{-0.011}	-0.0096 ^{+0.0029} _{-0.0039}	-0.0021 \pm 0.0020	-0.0042 ^{+0.0030} _{-0.0020}
M	0.826 ^{+0.034} _{-0.072}	0.919 ^{+0.015} _{-0.012}	0.9040 ^{+0.0038} _{-0.0089}	0.861 ^{+0.013} _{-0.029}	0.922 ^{+0.010} _{-0.004}	0.8958 ^{+0.0029} _{-0.0032}	0.9045 ^{+0.0043} _{-0.0098}
$\ln(10^{10} A_s)$	3.027 \pm 0.017	3.033 \pm 0.016	3.042 \pm 0.015	3.027 ^{+0.017} _{-0.015}	3.037 \pm 0.016	3.043 \pm 0.016	3.042 \pm 0.016
n_s	0.9710 \pm 0.0046	0.9681 \pm 0.0046	0.9664 \pm 0.0046	0.9707 \pm 0.0047	0.9683 \pm 0.0045	0.9636 \pm 0.0045	0.9661 \pm 0.0045
H_0 [km/s/Mpc]	58.2 ^{+1.3} _{-4.8}	76.2 ^{+2.3} _{-4.2}	72.96 ^{+0.59} _{-0.76}	60.2 ^{+0.2} _{-3.6}	73.4 \pm 1.3	72.80 \pm 0.55	73.19 ^{+0.56} _{-0.69}
σ_8	0.818 ^{+0.013} _{-0.043}	0.894 ^{+0.018} _{-0.028}	0.880 ^{+0.010} _{-0.015}	0.835 ^{+0.009} _{-0.029}	0.906 ^{+0.019} _{-0.013}	0.8743 \pm 0.0093	0.881 ^{+0.010} _{-0.016}
S_8	0.969 ^{+0.041} _{-0.031}	0.807 ^{+0.022} _{-0.020}	0.832 \pm 0.014	0.955 ^{+0.025} _{-0.020}	0.849 \pm 0.019	0.831 \pm 0.013	0.830 ^{+0.014} _{-0.015}
Ω_m	0.426 ^{+0.064} _{-0.031}	0.245 ^{+0.025} _{-0.017}	0.2681 ^{+0.0057} _{-0.0049}	0.395 ^{+0.043} _{-0.005}	0.2635 \pm 0.0098	0.2712 \pm 0.0045	0.2665 ^{+0.0053} _{-0.0047}
χ_{bf}^2	2762.79	2778.62	2787.06	3801.45	2764.02	3854.88	2787.57
$\Delta\chi_{\text{bf}}^2$	+2.70	+2.56	+10.08	-5.77	-18.98	+40.40	-5.90

B. BAO and SN Constraining Power

In Fig. 2 we see a CMB+SN confidence contour disjoint from CMB+BAO, and in Fig. 4 we see in addition multi-peaked 1D PDFs. It is worthwhile understanding their origin and effects. First, we emphasize that all chains are well converged, with $R - 1 < 0.02$, so these are real features of the posteriors.

The issue can be traced back to the CMB constraints, so it is not due to SN. The CMB carries cosmological information in three main characteristics: the geometric degeneracy to the last scattering surface (location of the acoustic peaks), the acoustic peak structure (influencing the baryon and cold dark matter constraints), and the integrated Sachs-Wolfe effect. In the VM noVEV model with curvature, and the VM VEV models both with and without curvature, there is sufficient freedom to prolong the matter domination era by raising Ω_m (compensating with Ω_k to preserve the geometric degeneracy) and thus suppress the ISW effect. This brings the lower ℓ multipoles into better agreement with CMB data. The intersection of the ISW suppression relation and geometric degeneracy in the M - Ω_m plane gives an opportunity for an extended CMB confidence contour, or second peak in the posterior.

For the VM noVEV model with curvature, the SN likelihood enhances the low ISW part of the confidence region because this also has larger Ω_m to offset the curvature for the SN distances. That is, the addition of the SN data chooses the far end of the CMB confidence region continuously connecting the two regions seen from CMB+SN and CMB+BAO. For the VM VEV cases the ISW suppression is stronger for the parameter region corresponding to the upper limit of M in Eq. (8), and this actually creates a second peak in the CMB posterior. Without the degeneracy due to curvature, the SN data is informative enough to nullify this second peak, just as BAO do, and so Fig. 3 shows CMB+BAO and CMB+SN in substantial agreement. However, again SN leverage is weakened in the presence of curvature and it is not able to remove the strongest part of the second posterior region from the CMB, giving rise to a disjoint second contour in Fig. 4. The unusual parameter values for CMB+SN in this case is due to the disjoint part of the CMB+SN posterior – the $H_0 \gtrsim 60$ disjoint part of the CMB+SN posterior has reasonable consistency with BAO data, e.g. with $H_0 \approx 72$, $\Omega_m \approx 0.27$. To highlight this we have italicized in Table V the entries involving Pantheon data to serve as a reminder that the values are the mean over both peaks in the posterior. Removing the $H_0 < 60$ contour peak, though, does not change χ_{bf}^2 for CMB+BAO+SN.

C. H_0 Results

As we have seen, the VM model can accommodate a high (R19) value of H_0 while being consistent with the CMB. Indeed the flat VM models have a better CMB χ^2 than Λ CDM, with the same number of parameters, while giving high H_0 . Including curvature, the VM models do about as well as Λ CDM+ Ω_k for CMB data, with greater uncertainties on H_0 but consistent with either low (Planck Λ CDM) or high values (the VM VEV curvature case for CMB alone has a peak at $H_0 \sim 70$ between the low and high values, as well as its main peak at $H_0 \sim 55$). These high values occur naturally, without adding an external H_0 prior.

Adding further data such as BAO and SN, or both, does not change the consistency with high H_0 (see the previous subsection for discussion of the CMB+SN data in the presence of curvature), although it can worsen (considerably)

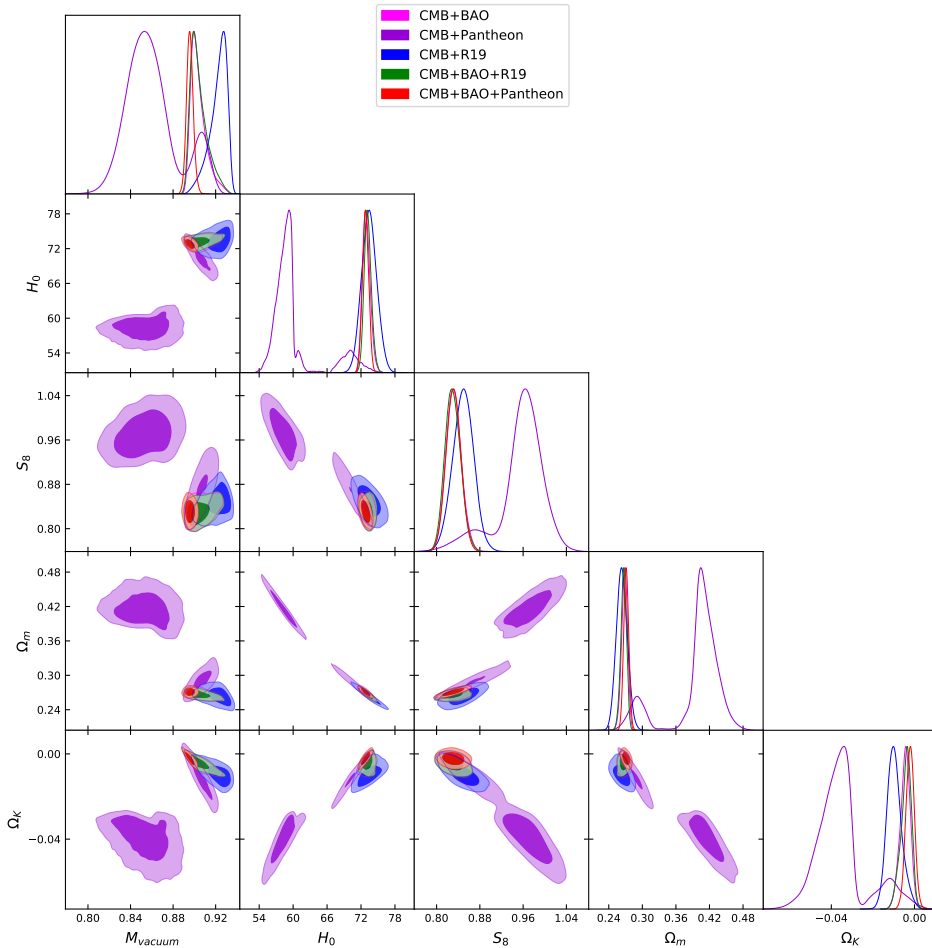


Figure 4. 68% and 95% CL constraints on the VM VEV case allowing spatial curvature to vary, i.e. VM VEV curvature.

the overall goodness of fit. Figure 5 shows the H_0 values fit for all the data combinations, for all the VM model permutations. However, as we caution in Sec. V, using only the criterion of a fit to H_0 can be highly problematic.

D. Ω_k Results

Evidence for nonzero spatial curvature, $\Omega_k \neq 0$, would have a profound impact on theories of the early universe and inflation. While we have seen that degeneracies with other parameters exist, and can increase uncertainties or easily allow large systematic shifts, the combination of many distinct observational probes can alleviate this. Furthermore, the VM model has the benefit of not increasing the number of parameters (and hence potential for further degeneracy) beyond Λ CDM (for VM noVEV; VM VEV has a single added parameter).

Earlier work, e.g. [67–71], has discussed evidence for (or against) a closed universe, $\Omega_k < 0$. However, these have considered only one or two probes together. Here we have several cases where we use three, either CMB+BAO+SN or CMB+BAO+R19. We do find that Ω_k tends to lie closer to zero when combining three probes than two, but the results still lie $\sim 3\sigma$ away from flatness for VM noVEV and $\sim 1\sigma$ away for the better fitting VM VEV.

Figure 6 shows the Ω_k values fit for all the data combinations, for all the VM model permutations. Again, we caution in Sec. V that one should consider the full set of cosmological model parameters together, rather than only focus on one. (For example, the CMB only Λ CDM+ Ω_k case that has an improvement of $\Delta\chi^2 = -11$ over flat Λ CDM also has $H_0 \approx 54$ and $\Omega_m \approx 0.48$; the VM VEV case is only slightly better, while the VM noVEV case is much closer to standard, both departing from flatness at $\sim 2-3\sigma$.)

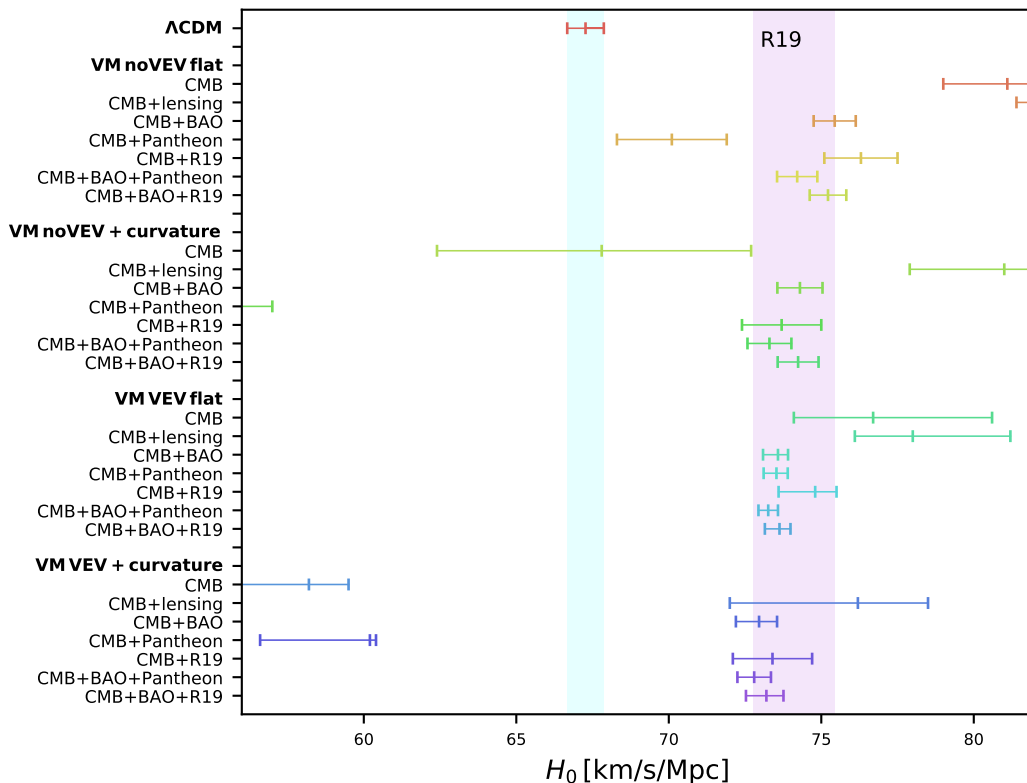


Figure 5. 68% CL constraints on H_0 for the different combinations of datasets and models explored here. The cyan region is the Planck Λ CDM estimate of the Hubble constant, while the violet region is the R19 measurement.

V. BEYOND H_0

As we have seen, for some of the VM models, while H_0 is in good agreement with R19 local measurements, and the CMB only data is well fit, the parameters associated with the matter density and structure growth are pushed away from the standard Λ CDM values. We explore the impact of this here, and show how the conjoined expansion-growth plots, e.g. as introduced in [72], can play an important role in assessing the overall fit of a model beyond just H_0 .

For example, focusing on the full data set combination CMB+BAO+SN, for Λ CDM the matter density takes values around $\Omega_m = 0.31$ while for the VM models it is $\Omega_m \approx 0.27$. The structure growth parameters are more difficult to assess, since the perturbation theory for the VM theory after the transition where the scalar curvature R freezes has not been calculated in detail (see [54] for a discussion of the difficulties). Thus, growth parameters such as σ_8 and S_8 should not be literally interpreted as values from the VM theory; however, they can be viewed as values for a dark energy theory with the same background expansion as VM (see Fig. 1 of [14] for the sharp transition of $w(z)$ to a phantom behavior). That is how we will interpret σ_8 and S_8 for the remainder of this section. The Monte Carlo runs of the previous section are robust since we chose data sets – CMB, BAO, and SN – that are predominantly geometric measures and insensitive to the behavior of the dark energy perturbations after the transition, $z \lesssim 1.5$.

Examining σ_8 in that light, we see a common characteristic of late time phantom transitions in dark energy: if they also seek to match the CMB, not just H_0 , then they tend to have higher σ_8 than Λ CDM. The extended era of matter domination, i.e. decreased dark energy density at redshifts $z \approx 0.5-2$, provides additional growth, increasing σ_8 . For VM-like expansion, σ_8 ranges from ~ 0.87 for the VM VEV expansion models to ~ 0.94 for VM noVEV expansion models, quite a bit above ~ 0.81 for Λ CDM. Note that early time dark energy models that raise H_0 by adding early energy density and hence decreasing the sound horizon scale, also generally raise σ_8 as well since they require a higher primordial curvature perturbation amplitude to offset the damping effect of the unclustered component. So both proposals for raising H_0 run into increased tension with values of σ_8 found from structure constraints.

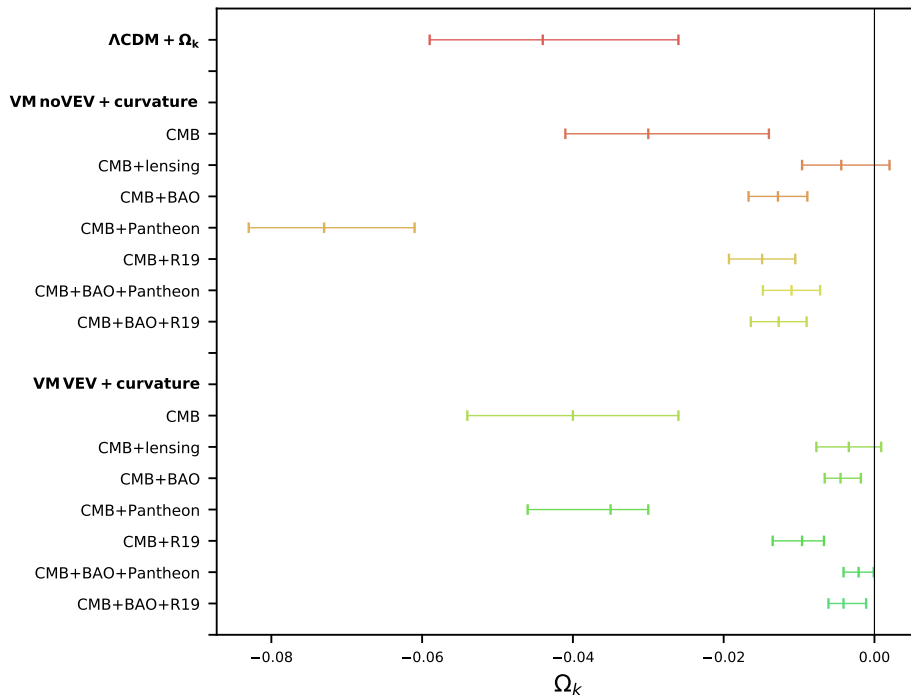


Figure 6. 68% CL constraints on Ω_k for the different combinations of datasets and models explored here.

However, many large scale structure surveys do not give σ_8 per se, but rather a quantity close to $S_8 \equiv \sigma_8 (\Omega_m/0.3)^{0.5}$. For example, this is the main degeneracy direction for many weak lensing shape measurements. This is also closely related to $f\sigma_8(z=0)$, central to galaxy clustering redshift space distortions, where $f = \Omega_m(a)^{0.55}$ is an excellent approximation to the growth rate even for many non- Λ CDM models [73–75]. So for S_8 , a redshift $z=0$ quantity,

$$S_8 = f\sigma_8(z=0) \times \left(\frac{1}{0.3}\right)^{0.55} \left(\frac{\Omega_m}{0.3}\right)^{-0.05} \approx 1.94 f\sigma_8(z=0). \quad (9)$$

Thus either weak lensing or redshift surveys give a quantity closer to S_8 . As we have seen, many of the models that give a higher H_0 give a lower Ω_m if they also match CMB data. We see that for VM-like expansion models, S_8 tends to be ~ 0.83 for the VM VEV cases, and ~ 0.88 for the VM noVEV cases, compared to ~ 0.82 for Λ CDM. Thus the VM VEV expansion cases give fairly good agreement with Λ CDM on this structure parameter. Of course some probes such as galaxy clusters and the Sunyaev-Zel’dovich effect do measure σ_8 more directly. We also must remember S_8 is simply the redshift $z=0$ value, and does not ensure that the growth history at $z=0.5$ or 1 is consistent with observational constraints.

What we want is a compact method for assessing the value of H_0 , the expansion history (as in CMB, BAO, and SN), and the growth history. This is often called a conjoined history diagram, highlighted in [72]. By plotting $f\sigma_8(z)$ directly against $H(z)$, with redshift running along the evolutionary tracks, one can not only see distinctions in dark energy properties such as equation of state, but modifications of gravity, or phenomenological effects from “stuttered” growth [72]. (Note that the superdeceleration leading to stuttered growth is precisely what is necessary for an early time dark energy transition to raise the value of H_0 without disrupting agreement with CMB data.)

Figure 7 presents the conjoint history diagram for Λ CDM and the various VM expansion models with the parameters given in the Monte Carlo results tables for CMB+BAO+SN. We see that if we look only at H_0 then the VM cases are well able to match the high value of H_0 . Even if we also look at $f\sigma_8(z=0)$ (or nearly equivalently S_8), the values can be quite close to Λ CDM. However, at higher redshift the conjoint history deviates sharply, and would not be consistent with data agreeing with Λ CDM. This emphasizes the need for a model to provide a good fit to *all* the data, not just one parameter. We have seen this in terms of the poor χ^2 in Sec. III and the conjoint history analysis provides another view of this.

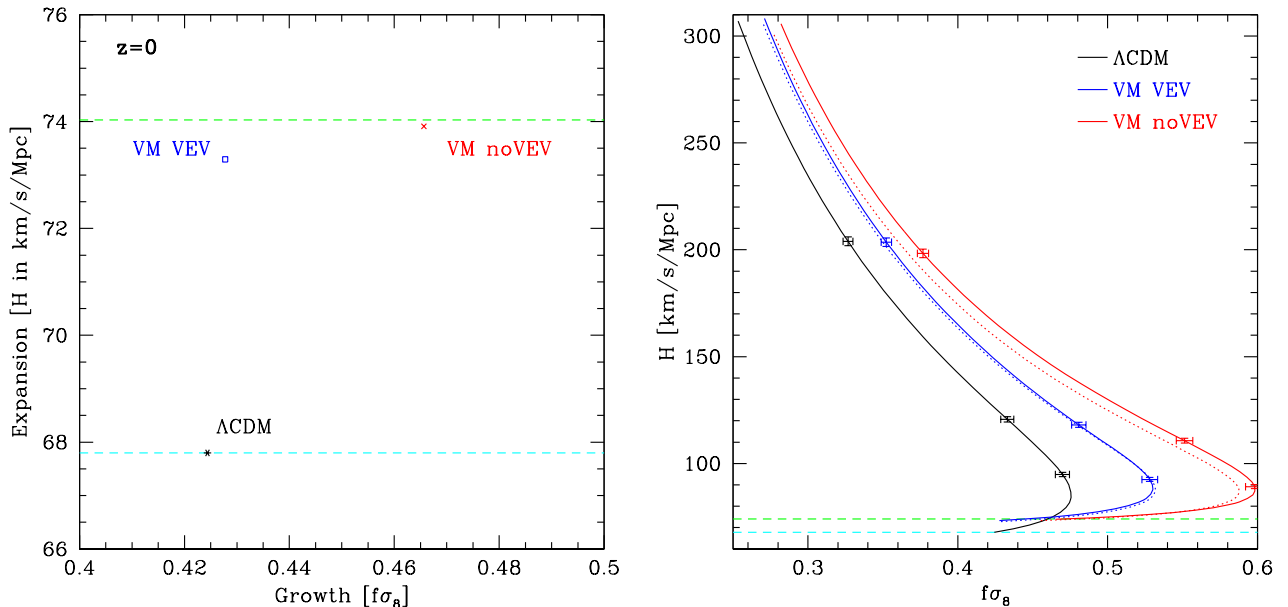


Figure 7. Expansion and growth histories are here plotted simultaneously. The left panel shows the situation looking only at $z = 0$, hence H_0 and $f\sigma_8(0)$ or effectively S_8 . Excellent agreement with the R19 value of H_0 (green dashed line), as opposed to the Λ CDM value (cyan dashed line) is obtained by the flat VEV models with parameters fit to CMB+BAO+SN, and the VM VEV model agrees well on S_8 as well. However, the right panel shows a very different situation if one looks beyond H_0 at the full conjoint evolutionary track of the various models, not just the $z = 0$ (lower) endpoints shown in the left panel. Over the histories the VM models diverge considerably from Λ CDM. Curves extend from $z = 0$ at the bottom to $z = 3$ at the top, and the points with error bars show the trajectory location at $z = 0.6, 1, 2$, where the error bars mimic 1% constraints on each axis quantity to give a sense of separation between the curves. Solid curves are for flat space, dotted curves include Ω_k , at the mean values from the results tables.

VI. DISCUSSION AND CONCLUSIONS

Obtaining a value of $H_0 \approx 74$ km/s/Mpc from the CMB is super easy, barely an inconvenience. Obtaining consistency when accounting for data sets from multiple cosmological probes – at a minimum including the recent universe, mid redshifts as seen by BAO and SN, and high redshift as evident in the CMB – and ideally both expansion and growth constraints, is not. Even then, while σ_8 or S_8 can provide a further critical test, these are simply the $z = 0$ value, and a more incisive test would be consistency in a conjoint analysis of both the expansion history and the growth history.

We demonstrate this with the vacuum metamorphosis model, a well motivated fundamental physics theory that has properties in common with many late time dark energy transition models. VM does quite well in fitting the CMB ($\Delta\chi^2 \approx -4.9$ to $+2.7$ with respect to Λ CDM, with the same or one more parameter), and in our baseline combination CMB+BAO+SN it achieves $H_0 \approx 73$ – 74 without using an H_0 prior, and gives comparable uncertainty to the Λ CDM case. However, for this three probe combination its goodness of fit is poor. That is, looking beyond just H_0 the theory fares poorly.

Such fit problems when taking into account the fuller array of data is common to many late time phantom dark energy transition attempts to attain $H_0 \gtrsim 70$ (see [76] for a clear illustration of the tension in CMB+BAO+SN when pushing into this phantom regime). Adding a vacuum expectation value to VM theory, i.e. VM VEV, delivers a strong improvement: $\Delta\chi^2 = -53$ for the one extra parameter, but still insufficient when considering the three probe combination. We also explore whether including spatial curvature could alleviate this, and indeed it can provide strong improvements for the CMB+SN case, but not for CMB+BAO+SN. Many data combinations prefer a closed universe, at 95% CL or greater, though for the better fitting VM VEV theory and the three probe combination, this is reduced to 68% CL.

Considering the amplitude of large scale structure, both late and early time transition models, by the nature of their mechanism for raising H_0 , also tend to raise σ_8 or S_8 above the Λ CDM value, which is already somewhat high with respect to observations. The VM VEV model (or its equivalent dark energy expansion behavior) can deliver $H_0 \approx 74$ and a similar S_8 to Λ CDM (though a higher σ_8). However, this is merely a snapshot at $z = 0$. We emphasize

the importance of a full conjoined analysis of the expansion and growth histories, by tracing $H(z)$ and $f\sigma_8(z)$ at mid redshifts as well.

In summary, if one has a very narrow focus, e.g. just on H_0 , then one can draw a very different conclusion regarding the attraction of models than if one properly takes into account the array of available data. H_0 *ex machina*, where a model swoops in to resolve a seemingly hopeless problem, can be intriguing, but given the array of cosmological data we want, and need, to go beyond H_0 . So far, neither early nor late time transitions have shown wholly viable solutions to the full cosmology.

ACKNOWLEDGMENTS

E.D.V. acknowledges support from the European Research Council in the form of a Consolidator Grant with number 681431. E.L. is supported in part by the Energetic Cosmos Laboratory and by the U.S. Department of Energy, Office of Science, Office of High Energy Physics, under Award DE-SC-0007867 and contract no. DE-AC02-05CH11231.

-
- [1] A. G. Riess, S. Casertano, W. Yuan, L. M. Macri, and D. Scolnic, *Astrophys. J.* **876**, 85 (2019), [arXiv:1903.07603 \[astro-ph.CO\]](#).
- [2] W. L. Freedman, B. F. Madore, T. Hoyt, I. S. Jang, R. Beaton, M. G. Lee, A. Monson, J. Neeley, and J. Rich, *Astrophys. J.* **891**, 57 (2020), [arXiv:2002.01550 \[astro-ph.GA\]](#).
- [3] N. Aghanim *et al.* (Planck), (2018), [arXiv:1807.06209 \[astro-ph.CO\]](#).
- [4] F. Bianchini *et al.* (SPT), *Astrophys. J.* **888**, 119 (2020), [arXiv:1910.07157 \[astro-ph.CO\]](#).
- [5] G. Addison, D. Watts, C. Bennett, M. Halpern, G. Hinshaw, and J. Weiland, *Astrophys. J.* **853**, 119 (2018), [arXiv:1707.06547 \[astro-ph.CO\]](#).
- [6] E. Macaulay *et al.* (DES), *Mon. Not. Roy. Astron. Soc.* **486**, 2184 (2019), [arXiv:1811.02376 \[astro-ph.CO\]](#).
- [7] A. Cuceu, J. Farr, P. Lemos, and A. Font-Ribera, *JCAP* **10**, 044 (2019), [arXiv:1906.11628 \[astro-ph.CO\]](#).
- [8] K. C. Wong *et al.*, (2019), [10.1093/mnras/stz3094](#), [arXiv:1907.04869 \[astro-ph.CO\]](#).
- [9] G. Efstathiou and J. Bond, *Mon. Not. Roy. Astron. Soc.* **304**, 75 (1999), [arXiv:astro-ph/9807103](#).
- [10] D. J. Eisenstein and M. J. White, *Phys. Rev. D* **70**, 103523 (2004), [arXiv:astro-ph/0407539](#).
- [11] M. Doran, S. Stern, and E. Thommes, *JCAP* **04**, 015 (2007), [arXiv:astro-ph/0609075](#).
- [12] E. V. Linder and G. Robbers, *JCAP* **06**, 004 (2008), [arXiv:0803.2877 \[astro-ph\]](#).
- [13] A. Hojjati, E. V. Linder, and J. Samsing, *Phys. Rev. Lett.* **111**, 041301 (2013), [arXiv:1304.3724 \[astro-ph.CO\]](#).
- [14] E. Di Valentino, E. V. Linder, and A. Melchiorri, *Phys. Rev. D* **97**, 043528 (2018), [arXiv:1710.02153 \[astro-ph.CO\]](#).
- [15] X. Li and A. Shafieloo, *Astrophys. J. Lett.* **883**, L3 (2019), [arXiv:1906.08275 \[astro-ph.CO\]](#).
- [16] S. Pan, W. Yang, E. Di Valentino, A. Shafieloo, and S. Chakraborty, (2019), [arXiv:1907.12551 \[astro-ph.CO\]](#).
- [17] X. Li and A. Shafieloo, (2020), [arXiv:2001.05103 \[astro-ph.CO\]](#).
- [18] N. Khosravi, S. Baghran, N. Afshordi, and N. Altamirano, *Phys. Rev. D* **99**, 103526 (2019), [arXiv:1710.09366 \[astro-ph.CO\]](#).
- [19] E. Di Valentino, A. Mukherjee, and A. A. Sen, (2020), [arXiv:2005.12587 \[astro-ph.CO\]](#).
- [20] V. Poulin, T. L. Smith, T. Karwal, and M. Kamionkowski, *Phys. Rev. Lett.* **122**, 221301 (2019), [arXiv:1811.04083 \[astro-ph.CO\]](#).
- [21] T. L. Smith, V. Poulin, and M. A. Amin, *Phys. Rev. D* **101**, 063523 (2020), [arXiv:1908.06995 \[astro-ph.CO\]](#).
- [22] P. Agrawal, F.-Y. Cyr-Racine, D. Pinner, and L. Randall, (2019), [arXiv:1904.01016 \[astro-ph.CO\]](#).
- [23] M.-X. Lin, G. Benevento, W. Hu, and M. Raveri, *Phys. Rev. D* **100**, 063542 (2019), [arXiv:1905.12618 \[astro-ph.CO\]](#).
- [24] F. Niedermann and M. S. Sloth, (2019), [arXiv:1910.10739 \[astro-ph.CO\]](#).
- [25] J. C. Hill, E. McDonough, M. W. Toomey, and S. Alexander, (2020), [arXiv:2003.07355 \[astro-ph.CO\]](#).
- [26] G. Benevento, W. Hu, and M. Raveri, *Phys. Rev. D* **101**, 103517 (2020), [arXiv:2002.11707 \[astro-ph.CO\]](#).
- [27] L. Knox and M. Millea, *Phys. Rev. D* **101**, 043533 (2020), [arXiv:1908.03663 \[astro-ph.CO\]](#).
- [28] E. Di Valentino, A. Melchiorri, O. Mena, and S. Vagnozzi, (2019), [arXiv:1908.04281 \[astro-ph.CO\]](#).
- [29] N. Arendse *et al.*, (2019), [arXiv:1909.07986 \[astro-ph.CO\]](#).
- [30] C. Garcia-Quintero, M. Ishak, L. Fox, and W. Lin, *Phys. Rev. D* **100**, 123538 (2019), [arXiv:1910.01608 \[astro-ph.CO\]](#).
- [31] L. Hart and J. Chluba, (2019), [arXiv:1912.03986 \[astro-ph.CO\]](#).
- [32] E. Di Valentino, A. Melchiorri, O. Mena, and S. Vagnozzi, (2019), [arXiv:1910.09853 \[astro-ph.CO\]](#).
- [33] M. Liu, Z. Huang, X. Luo, H. Miao, N. K. Singh, and L. Huang, *Sci. China Phys. Mech. Astron.* **63**, 290405 (2020), [arXiv:1912.00190 \[astro-ph.CO\]](#).
- [34] M. M. Ivanov, M. Simonović, and M. Zaldarriaga, *Phys. Rev. D* **101**, 083504 (2020), [arXiv:1912.08208 \[astro-ph.CO\]](#).
- [35] J. Alcaniz, N. Bernal, A. Masiero, and F. S. Queiroz, (2019), [arXiv:1912.05563 \[astro-ph.CO\]](#).
- [36] N. Frusciante, S. Peirone, L. Atayde, and A. De Felice, (2019), [arXiv:1912.07586 \[astro-ph.CO\]](#).
- [37] W. Yang, E. Di Valentino, S. Pan, S. Basilakos, and A. Paliathanasis, (2020), [arXiv:2001.04307 \[astro-ph.CO\]](#).
- [38] K. Jedamzik and L. Pogosian, (2020), [arXiv:2004.09487 \[astro-ph.CO\]](#).

- [39] S. Pan, G. S. Sharov, and W. Yang, (2020), [arXiv:2001.03120 \[astro-ph.CO\]](#).
- [40] W. K. Wu, P. Motloch, W. Hu, and M. Raveri, (2020), [arXiv:2004.10207 \[astro-ph.CO\]](#).
- [41] G. Ye and Y.-S. Piao, (2020), [arXiv:2001.02451 \[astro-ph.CO\]](#).
- [42] M. Braglia, M. Ballardini, W. T. Emond, F. Finelli, A. E. Gumrukcuoglu, K. Koyama, and D. Paoletti, (2020), [arXiv:2004.11161 \[astro-ph.CO\]](#).
- [43] N. Blinov and G. Marques-Tavares, (2020), [arXiv:2003.08387 \[astro-ph.CO\]](#).
- [44] D. Wang and D. Mota, (2020), [arXiv:2003.10095 \[astro-ph.CO\]](#).
- [45] A. Chudaykin, D. Gorbunov, and N. Nedelko, (2020), [arXiv:2004.13046 \[astro-ph.CO\]](#).
- [46] G. Alestas, L. Kazantzidis, and L. Perivolaropoulos, *Phys. Rev. D* **101**, 123516 (2020), [arXiv:2004.08363 \[astro-ph.CO\]](#).
- [47] S. J. Clark, K. Vattis, and S. M. Koushiappas, (2020), [arXiv:2006.03678 \[astro-ph.CO\]](#).
- [48] M. Ballardini, M. Braglia, F. Finelli, D. Paoletti, A. A. Starobinsky, and C. Umiltà, (2020), [arXiv:2004.14349 \[astro-ph.CO\]](#).
- [49] R. E. Keeley, A. Shafieloo, D. K. Hazra, and T. Souradeep, (2020), [arXiv:2006.12710 \[astro-ph.CO\]](#).
- [50] F. Niedermann and M. S. Sloth, (2020), [arXiv:2006.06686 \[astro-ph.CO\]](#).
- [51] M. Archidiacono, S. Gariazzo, C. Giunti, S. Hannestad, and T. Tram, (2020), [arXiv:2006.12885 \[astro-ph.CO\]](#).
- [52] L. Parker and A. Raval, *Phys. Rev. D* **62**, 083503 (2000), [Erratum: *Phys.Rev.D* 67, 029903 (2003)], [arXiv:gr-qc/0003103](#).
- [53] L. Parker and D. A. Vanzella, *Phys. Rev. D* **69**, 104009 (2004), [arXiv:gr-qc/0312108](#).
- [54] R. R. Caldwell, W. Komp, L. Parker, and D. A. Vanzella, *Phys. Rev. D* **73**, 023513 (2006), [arXiv:astro-ph/0507622](#).
- [55] A. A. Starobinsky, *Adv. Ser. Astrophys. Cosmol.* **3**, 130 (1987).
- [56] A. Sakharov, *Usp. Fiz. Nauk* **161**, 64 (1991).
- [57] N. Aghanim *et al.* (Planck), (2019), [arXiv:1907.12875 \[astro-ph.CO\]](#).
- [58] N. Aghanim *et al.* (Planck), (2018), [arXiv:1807.06210 \[astro-ph.CO\]](#).
- [59] F. Beutler, C. Blake, M. Colless, D. Jones, L. Staveley-Smith, L. Campbell, Q. Parker, W. Saunders, and F. Watson, *Mon. Not. Roy. Astron. Soc.* **416**, 3017 (2011), [arXiv:1106.3366 \[astro-ph.CO\]](#).
- [60] A. J. Ross, L. Samushia, C. Howlett, W. J. Percival, A. Burden, and M. Manera, *Mon. Not. Roy. Astron. Soc.* **449**, 835 (2015), [arXiv:1409.3242 \[astro-ph.CO\]](#).
- [61] S. Alam *et al.* (BOSS), *Mon. Not. Roy. Astron. Soc.* **470**, 2617 (2017), [arXiv:1607.03155 \[astro-ph.CO\]](#).
- [62] D. Scolnic *et al.*, *Astrophys. J.* **859**, 101 (2018), [arXiv:1710.00845 \[astro-ph.CO\]](#).
- [63] A. Lewis and S. Bridle, *Phys. Rev. D* **66**, 103511 (2002), [arXiv:astro-ph/0205436](#).
- [64] A. Gelman and D. B. Rubin, *Statist. Sci.* **7**, 457 (1992).
- [65] A. Lewis, *Phys. Rev. D* **87**, 103529 (2013), [arXiv:1304.4473 \[astro-ph.CO\]](#).
- [66] D. Rubin *et al.*, *Astrophys. J.* **695**, 391 (2009), [arXiv:0807.1108 \[astro-ph\]](#).
- [67] W. Handley, (2019), [arXiv:1908.09139 \[astro-ph.CO\]](#).
- [68] E. Di Valentino, A. Melchiorri, and J. Silk, *Nature Astron.* **4**, 196 (2019), [arXiv:1911.02087 \[astro-ph.CO\]](#).
- [69] G. Efstathiou and S. Gratton, *Mon. Not. Roy. Astron. Soc.* **496**, L91 (2020), [arXiv:2002.06892 \[astro-ph.CO\]](#).
- [70] K. Liao, A. Shafieloo, R. E. Keeley, and E. V. Linder, *Astrophys. J.* **895**, L29 (2020), [arXiv:2002.10605 \[astro-ph.CO\]](#).
- [71] E. Di Valentino, A. Melchiorri, and J. Silk, (2020), [arXiv:2003.04935 \[astro-ph.CO\]](#).
- [72] E. V. Linder, *Astropart. Phys.* **86**, 41 (2017), [arXiv:1610.05321 \[astro-ph.CO\]](#).
- [73] E. V. Linder, *Phys. Rev. D* **72**, 043529 (2005), [arXiv:astro-ph/0507263 \[astro-ph\]](#).
- [74] E. V. Linder and R. N. Cahn, *Astroparticle Physics* **28**, 481 (2007), [arXiv:astro-ph/0701317 \[astro-ph\]](#).
- [75] L. Wang and P. J. Steinhardt, *Astrophys. J.* **508**, 483 (1998), [arXiv:astro-ph/9804015 \[astro-ph\]](#).
- [76] E. Di Valentino, A. Melchiorri, E. V. Linder, and J. Silk, *Phys. Rev. D* **96**, 023523 (2017), [arXiv:1704.00762 \[astro-ph.CO\]](#).